

Controlling Self-Assembly in Gyroid Terpolymer Films By Solvent Vapor Annealing

James A. Dolan, Karolina Korzeb, Raphael Dehmel, Karl C. Gödel, Morgan Stefik, Ulrich Wiesner, Timothy D. Wilkinson, Jeremy J. Baumberg, Bodo D. Wilts, Ullrich Steiner, and Ilja Gunkel*

The efficacy with which solvent vapor annealing (SVA) can control block copolymer self-assembly has so far been demonstrated primarily for the simplest class of copolymer, the linear diblock copolymer. Adding a third distinct block—thereby creating a triblock terpolymer—not only provides convenient access to complex continuous network morphologies, particularly the gyroid phases, but also opens up a route toward the fabrication of novel nanoscale devices such as optical metamaterials. Such applications, however, require the generation of well-ordered 3D continuous networks, which in turn requires a detailed understanding of the SVA process in terpolymer network morphologies. Here, *in situ* grazing-incidence small-angle X-ray scattering (GISAXS) is employed to study the self-assembly of a gyroid-forming triblock terpolymer during SVA, revealing the effects of several key SVA parameters on the morphology, lateral order, and, in particular, its preservation in the dried film. The robustness of the terpolymer gyroid morphology is a key requirement for successful SVA, allowing the exploration of annealing parameters which may enable the generation of films with long-range order, e.g., for optical metamaterial applications.

process, and it is often advantageous to utilize solvent vapor annealing (SVA). Compared to thermal annealing, the introduction of controlled amounts of a suitable solvent greatly increases the mobility of the BCP, thereby reducing the timescale of self-assembly,^[8] which is essential for generating order especially in high molecular weight BCPs.^[9,10] By carefully tuning the amount of solvent and its subsequent removal, it is possible to substantially increase the resulting size of the self-assembled grains.^[11–14]

The effect of SVA on linear diblock copolymers is well understood.^[15,16] In the ideal case of a nonselective good solvent, both blocks of the copolymer swell equally, leaving the effective volume fractions of the blocks f_A and f_B unaltered, but screening the interaction between the two blocks (i.e., lowering the Flory–Huggins interaction parameter χ_{AB}). A sufficiently high solvent concentration lowers χ_{AB} to such an extent that the microphase-separated morphology

is no longer thermodynamically favorable and the copolymer forms a disordered phase. A selective solvent, on the other hand, preferentially swells one of the blocks, altering the effective volume fractions and thereby influencing the equilibrium morphology of the swollen copolymer.^[17–20] It is thus possible to explore the entire phase space of diblock copolymers (i.e., spheres, cylinders, the double gyroid and lamellae) with only a single copolymer by varying the solvent concentration and selectivity.^[18]

1. Introduction

Block copolymer (BCP) self-assembly is a particularly promising route to fabricate functional nanomaterials over macroscopically large areas.^[1] For many applications, long-range order on the millimeter length scale is required, e.g., for 1D and 2D nanolithographic templates,^[2–4] and 3D optical metamaterials.^[5–7] Producing BCP films with such high degrees of order requires an annealing

Dr. J. A. Dolan,^[†] Dr. R. Dehmel,^[††] Dr. K. C. Gödel,^[†††] Prof. J. J. Baumberg
Department of Physics
University of Cambridge
J.J. Thomson Avenue, Cambridge CB3 0HE, UK

 The ORCID identification number(s) for the author(s) of this article can be found under <https://doi.org/10.1002/sml.201802401>.

^[†]Present address: Institute for Molecular Engineering, Argonne National Laboratory, 9700 S. Cass Avenue, Argonne, IL 60439, USA

^[††]Present address: Papierfabrik Louisenthal GmbH, 83701 Gmund a.T., Germany

^[†††]Present address: Robert Bosch GmbH, Maybachstraße 6, 70469 Stuttgart, Germany

DOI: 10.1002/sml.201802401

Dr. J. A. Dolan, Prof. T. D. Wilkinson
Department of Engineering
University of Cambridge
Cambridge CB2 1PZ, UK

Dr. J. A. Dolan, K. Korzeb, Dr. B. D. Wilts, Prof. U. Steiner, Dr. I. Gunkel
Adolphe Merkle Institute
Chemin des Verdiers, CH-1700 Fribourg, Switzerland
E-mail: ilja.gunkel@unifr.ch

Prof. M. Stefik
Department of Chemistry and Biochemistry
University of South Carolina
541 Main St, Horizon I BLDG, Columbia, SC 29208, USA

Prof. U. Wiesner
Department of Materials Science and Engineering
Cornell University
214 Bard Hall, Ithaca, NY 14853, USA

When using diblock copolymers, the double gyroid morphology forms only in a relatively small range of the copolymer's composition, which makes the control of grain coarsening difficult because of the sensitivity with respect to undesired morphological transitions. This hinders efforts to improve the long-range order in the only 3D interconnected diblock copolymer morphology, i.e., the double gyroid. She et al. demonstrated the controlled ordering of the double gyroid morphology in diblock copolymer thin films upon annealing in a neutral solvent and employing a functionalized substrate.^[21] Similarly, Wu et al. explored the effect of swollen thickness and solvent removal rate on the resulting morphology of solvent-annealed gyroid-forming diblock copolymers.^[22] Both publications report, however, morphological transitions to the cylinder phase, despite the use of a supposedly neutral solvent. Coexisting spherical and gyroid morphologies were also observed, further demonstrating the difficulty of retaining the gyroid phase in diblock copolymer swollen melts during SVA, impeding the improvement of long-range order in this system.^[18]

It is well known that triblock terpolymers form 3D interconnected morphologies for much wider block-composition ranges than diblock copolymers.^[23,24] For example, the double gyroid (Q^{230}) in bulk polyisoprene-*b*-polystyrene (PI-*b*-PS) diblock copolymers forms for $0.36 < f_{PI} < 0.39$ and $0.65 < f_{PI} < 0.69$,^[25,26] while its core-shell counterpart (also Q^{230}) in bulk polyisoprene-*b*-polystyrene-*b*-poly(ethylene oxide) (ISO) triblock terpolymers forms for $f_{PI}/f_{PS} = 1.38$, $0.14 < f_{PEO} < 0.20$, and $f_{PI}/f_{PS} = 1.27$, $0.11 < f_{PEO} < 0.20$.^[24,27,28] The alternating gyroid (Q^{214}) in bulk ISO terpolymers shows a similarly large composition range: $f_{PI}/f_{PS} = 0.64$, $0.14 < f_{PEO} < 0.18$ and $f_{PI}/f_{PS} = 0.45$, $0.17 < f_{PEO} < 0.29$.^[24,27,28]

For functionalities that benefit from ordered gyroid phases, it is therefore advantageous to induce long-range lateral order by means of SVA in triblock terpolymers rather than diblock copolymers. In this system, it should be possible to maintain the chosen gyroid morphology during solvent uptake even for changes in the volume fractions of the three blocks caused by solvent selectivity. The study of morphological evolution of linear triblock copolymers (ABA) and terpolymers (ABC) during SVA has, by comparison, received relatively little attention, and SVA of gyroid-forming triblock copolymers or terpolymers has only very recently been investigated at all. Previous studies on ABA triblock copolymers focused instead on the morphological transitions resulting from the exposure to selective and neutral solvents,^[29] the improvement in symmetry and long-range order of the cylindrical and lamellar microphase-separated morphologies,^[29] and the effect of the solvent evaporation rate on the orientation of cylindrical domains.^[30–32] Early studies on ABC triblock copolymer films investigated the effect of solvent,^[33] solvent removal rate,^[33,34] and annealing time^[35] upon morphology and domain orientation. Only recently, Antoine et al. studied *ex situ* the SVA of a core-shell double gyroid-forming ABC triblock terpolymer, and Aissou et al. the SVA of an alternating gyroid-forming ABC triblock, demonstrating reorientation and morphological transitions in thin (sub-200 nm) films.^[36,37]

In this work, we used grazing-incidence small-angle X-ray scattering (GISAXS) to study the kinetics and thermodynamics of a linear, alternating gyroid-forming ISO triblock terpolymer

during SVA. GISAXS is the most direct means to study block copolymer morphologies *in situ* during SVA, allowing the simultaneous characterization of both in- and out-of-plane electron density correlations over macroscopically large areas in real time.^[12,17–20,38–42] We annealed ISO terpolymer films in the mixed vapors of tetrahydrofuran (THF) and methanol of various compositions, and identified the degree of in- and out-of-plane order of the resulting gyroid morphology upon varying the maximum solvent concentration and solvent removal rate.

2. Results

To study the kinetics and thermodynamics of the ISO triblock terpolymer during SVA, thin films of the terpolymer were exposed to controlled solvent vapor atmospheres while the resulting film thickness and GISAXS scattering patterns were recorded at regular intervals. SVA regimes were identified by tracking the GISAXS scattering patterns and the associated peak metrics (i.e., the position and width) as a function of swelling ratio. The presence and behavior of peaks reveal the effect of the solvent on the film. After swelling the films to a maximum swelling ratio, they were quenched in a nitrogen flow at a well defined quench rate, and the resulting microphase-separated morphology and degree of order in the resulting dried films were investigated. Finally, the effect of the solvent vapor composition—and therefore the varying selectivity of the solvents for the individual blocks of the terpolymer—was similarly studied.

All studied solvent-annealed films exhibited the alternating gyroid microphase-separated morphology. This morphology was assigned based on 2D indexing of the GISAXS scattering patterns (**Figure 1**). Figure 1a shows the successfully indexed GISAXS scattering pattern of an ISO film swollen with the mixed vapors THF and methanol (flow rate ratio 80:20). The indexed peaks are labeled in Figure 1b. The peaks observed in the scattering pattern, which is typical for all patterns observed in this study, clearly agree excellently with the expected peaks of the $I4_132$ (single gyroid; Q^{214}) space group, indicative of the alternating gyroid morphology. The [110] direction was oriented perpendicular to the substrate in all studied films. The unit cell parameters ($a = b = 35.8$ nm, $c = 34.9$ nm, and $\gamma = 89^\circ$) reveal a slight (sub-nanometer) deviation from the gyroid cubic symmetry in the out-of-plane [110] direction; the unit cell parameters, but not the morphology, can vary substantially as a function of SVA parameters (see below). Figure 1c shows a representative atomic force microscopy (AFM) image of an ISO film after annealing in the mixed vapors of THF and methanol (80:20) and subsequent quenching according to the protocol applied to the film shown in Figure 3d. The film surface features a regular dot array that corresponds well to the (110) surface plane of a body-centered cubic (BCC) lattice with a lateral unit cell size $a = 34.5$ nm, as determined by the fast Fourier transform (FFT) of the image. This plane is both qualitatively and quantitatively consistent with the indexed single gyroid morphology. The alternating gyroid morphology of the ISO terpolymer, consisting of two enantiomorphic single gyroid networks of PI ($f_{PI} = 0.31$) and polyethylene oxide (PEO) ($f_{PEO} = 0.17$), is shown in Figure 1d.

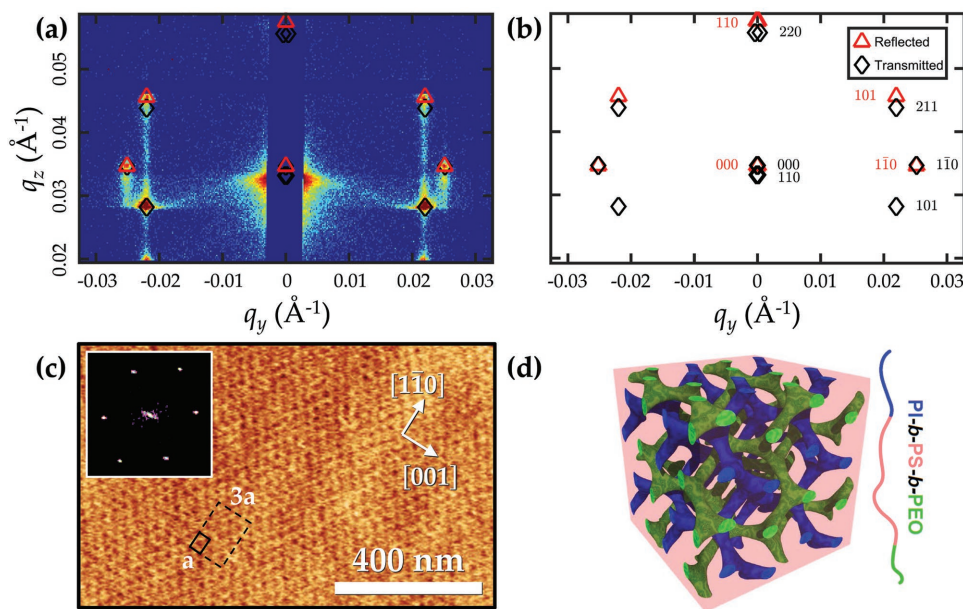


Figure 1. Alternating gyroid microphase-separated morphology. The alternating gyroid morphology with the I_4132 (single gyroid; Q^{214}) space group was identified in all swollen and dried ISO films. a) GISAXS scattering pattern of an ISO film swollen in the mixed vapors of THF and methanol (80:20), indexed with first and second order peaks of the I_4132 space group with the $[110]$ direction oriented perpendicular to the substrate and the unit cell parameters $a = b = 35.8$ nm, $c = 34.9$ nm, and $\gamma = 89^\circ$. b) Corresponding peak labels highlighting the “reflected” (red triangles) and “transmitted” (black diamonds) peak positions.^[44] c) Atomic force microscopy (AFM) amplitude image of the (110) surface of a dried ISO film after annealing in the mixed vapors of THF and methanol (80:20). A unit cell is indicated with a black rectangle. The average periodicities along the $[001]$ and $[110]$ directions (indicated), extracted using the FFT (inset) of the amplitude image, are 34.5 and 46.2 nm, respectively. d) Schematic of the alternating gyroid morphology formed by the ISO triblock terpolymer.

2.1. Solvent Vapor Annealing Regimes

Different SVA morphological regimes were identified in the ISO films by observing changes in the scattering patterns as a function of the swelling ratio ϕ , i.e., the ratio of the swollen to dried film thickness (see the Experimental Section). **Figure 2** shows the eight regimes identified during the swelling and deswelling of an ISO film in the mixed vapors of THF and methanol (80:20). As readily determined by homopolymer dissolution experiments, THF is a good solvent for PS, PI, and PEO; methanol is a good solvent only for PEO (better than THF) and a poor solvent for PS and PI. A THF-rich mixture of the two solvent vapors, as used here, is therefore anticipated to be a good solvent for all ISO blocks. More specifically, Figure 2 shows the GISAXS scattering patterns (Figure 2a), swelling ratios (Figure 2b), line integral surfaces (Figure 2c), and in-plane scattering peak metrics (Figure 2d,e) corresponding to the eight SVA regimes. The variation of the line integral surfaces with swelling ratio corresponds to in-plane variations of the $[1\bar{1}0]$ peaks at their out-of-plane wave vector $q_z^{[1\bar{1}0]}$ (cf. Figure 1). The scattering peak metrics show the variation of the position of the $[1\bar{1}0]$ peak $q_y^{[1\bar{1}0]} \approx 0.026 \text{ \AA}^{-1}$ (Figure 2d) and width $\Delta q_y^{[1\bar{1}0]}$ (Figure 2e) during swelling and deswelling in the ordered regimes, calculated from the GISAXS line integrals. The eight SVA regimes and their corresponding onset swelling ratios^[43] are identified as follows:

i) *As-Spun*: After spin-coating and before application of solvent vapor ($\phi = 1.00$), the GISAXS scattering pattern exhibits

significant intensity along the entirety of the “diffuse Debye–Scherrer ring” (DDSR) spanning the entirety of the $q_y q_z$ plane at $q_y \approx \pm 0.025$ and $q_z \approx 0.04 \text{ \AA}^{-1}$.^[44] This high intensity DDSR includes contributions from both the “reflected” and “transmitted” beams and appears as a broad single peak in the line integral surface (cf. Figure 1).^[44] The significant presence of a DDSR is indicative of a poorly ordered isotropic microphase-separated morphology.

ii) *Plasticization*: As the solvent concentration in the film increases ($\phi \approx 1.10$), the GISAXS pattern begins to change. The locus of the high intensity DDSR shifts to lower q_z values. This indicates plasticization of the polymer (i.e., a lowering of the glass transition temperature of the PS matrix T_g^{PS} below ambient temperature) and relaxation of the as-spun morphology.

iii) *Ordering*: As the solvent concentration in the film is increased ($\phi \approx 1.29$), the intensity of the DDSR reduces and distinct Bragg reflections begin to appear. Similarly, the line integral surface begins to exhibit two laterally separate signals, labeled P_1 and P_2 . The P_1 signal is associated with the reflected and transmitted $[101]$ and transmitted $[211]$ peaks of the alternating gyroid morphology; the P_2 signal is associated with the reflected and transmitted $[1\bar{1}0]$ peaks, i.e., $q_y^{[1\bar{1}0]}$ (cf. Figure 1). The appearance of distinct Bragg reflections indicates the onset of ordering in the polymer film.

iv) *Order*: With a further increase in solvent concentration ($\phi \approx 1.39$), the DDSR disappears and distinct, pronounced Bragg reflections appear at $q_y \approx \pm 0.023$ and $q_z \approx \pm 0.026 \text{ \AA}^{-1}$. The peak metrics corresponding to P_2 in Figure 2d,e exhibit

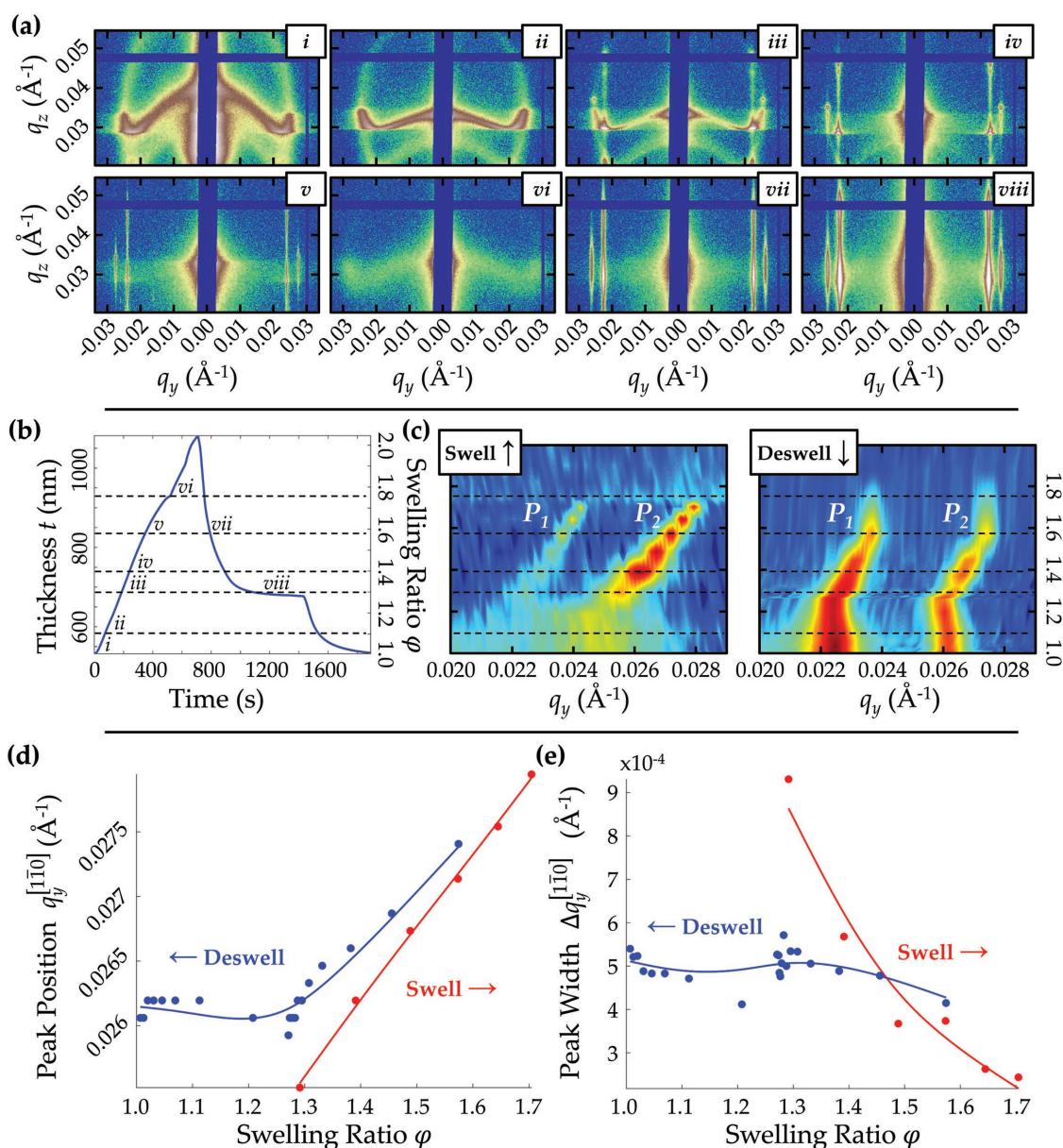


Figure 2. Solvent vapor annealing (SVA) regimes during swelling and deswelling of an ISO film. Eight SVA regimes were identified during the swelling and deswelling of an ISO film in the mixed vapors of THF and methanol (80:20). a) Representative GISAXS patterns for the eight SVA regimes, acquired at a fixed angle of incidence ($\alpha_i = 0.18^\circ$). The regimes and corresponding swelling ratios (ϕ) are labeled as: *i*) as-spun (1.00); *ii*) plasticization (1.10); *iii*) ordering (1.29); *iv*) order (1.39); *v*) approaching disorder (1.57); *vi*) disorder (1.74); *vii*) reordering (1.57); and *viii*) vitrification (1.29). The logarithmic color scales were normalized to the maximum and minimum intensities of each pattern. b) Film thickness and swelling ratio as a function of time. c) Swelling and deswelling line integral surfaces: the line integral of the GISAXS pattern at the out-of-plane wave vector $q_z^{[110]}$ is plotted as a function of swelling ratio (cf. Figure 1). The logarithmic color scales were normalized to the maximum and minimum intensities of each complete set of line integrals. d) Peak position $q_y^{[110]}$ and e) width $\Delta q_y^{[110]}$ (full width at half maximum) of the peak at $q_y \approx 0.026 \text{ \AA}^{-1}$ (P_2) during swelling (red) and deswelling (blue). The peak metrics were calculated from the GISAXS line integrals. The solid lines are guides to the eye.

an increase in $q_y^{[110]}$ and reduction in $\Delta q_y^{[110]}$, respectively, with increasing solvent concentration. The disappearance of the DDSR and the increased intensity of the Bragg reflections indicate that the copolymer has assembled into a well-ordered morphology that is consistent with the alternating gyroid (cf. Figure 1). The increase in $q_y^{[110]}$ with swelling ratio and the reduction in $\Delta q_y^{[110]}$ indicate a slight decrease in the gyroid lateral unit cell size with increasing long-range order.

v) **Approaching Disorder.** Upon further increase in solvent concentration ($\phi \approx 1.57$), the distinct signal variation in q_z for the Bragg reflections at $q_y \approx \pm 0.023 \text{ \AA}^{-1}$ and $q_y \approx \pm 0.026 \text{ \AA}^{-1}$ smear-out into “diffuse Bragg rods.” Interestingly, the quality of the in-plane order continues to increase, witnessed by a decrease in $\Delta q_y^{[110]}$ in Figure 2e. The narrowing of the in-plane reflection peaks indicates, on the one hand, the continued presence and improved ordering of the gyroid morphology in at

least part of the film, evident when probed over large in-plane areas. The loss of distinct out-of-plane peaks into Bragg rods indicates, on the other hand, a loss of the periodic morphology spanning across the entire thickness of the film, which may arise from interfacial disorder, as discussed below.

- vi) **Disorder:** Approaching the highest explored solvent concentration of $\varphi \approx 1.74$, the diffuse Bragg rods disappear and only a very faint DDSR is visible in the GISAXS patterns, reducing the line integral surface to zero. The disappearance of the Bragg rods indicates the absence of a microphase-separated morphology, i.e., disorder, and the occurrence of a transition to a disordered phase similar to the lyotropic order–disorder transitions observed in block copolymers in (selective) solvents.^[45]
- vii) **Reordering:** As the solvent concentration is decreased ($\varphi \approx 1.57$), the diffuse Bragg rods at $q_y \approx \pm 0.023$ and $q_y \approx \pm 0.026 \text{ \AA}^{-1}$ begin to reappear in the GISAXS pattern and the deswelling line integral surface. The peak $P_2 \sim q_y^{[110]}$ reduces in its q_y value on a trajectory similar to that during swelling and broadens slightly. The reappearance of the Bragg rods indicates that the terpolymer has begun to self-assemble towards its equilibrium microphase-separated morphology. The peak metrics indicate that the lateral unit cell is slightly increased and the degree of order is lower compared to regime vi.
- viii) **Vitrification:** As the solvent concentration is further decreased ($\varphi \approx 1.29$), the diffuse Bragg rods increase in intensity and the $P_2 \sim q_y^{[110]}$ peak remains at a stationary q_y value and peak width. The GISAXS pattern, deswelling line integral surface, and peak metrics do not change any further as remaining solvent is removed. The stability of the peak metrics indicates the vitrification of at least one of the copolymer domains (almost certainly the PS), immobilizing the entire terpolymer morphology. For high T_g polymers, vitrification typically sets in at substantial swelling ratios.

2.2. Effect of the Maximum Swelling Ratio and Solvent Removal Rate

Having identified the various regimes observed during SVA of ISO films, the SVA parameter space was explored with the aim of maintaining the highly ordered state of the swollen microphase-separated morphology (i.e., regime iv in Figure 1a) in the dried film. To this end, the coupled effect of quenching the film from either the disordered regime (close to disorder) or the ordered regime (determined by the maximum swelling ratio), and the rate of solvent removal, were investigated. **Figure 3** shows four SVA protocols together with GISAXS scattering patterns in the swollen and dried states. The mixed solvent vapors of THF and methanol (80:20) were used.

2.2.1. Maximum Swelling Ratio

Three different maximum swelling ratios were chosen. The two films marked in blue in Figure 3a were swollen to $\varphi_{\max} \approx 1.6$ and 2.0, closely below and well above the order–disorder transition, respectively, as confirmed by the GISAXS patterns of the maximally swollen films in Figure 3b,c. Only the film

swollen to $\varphi_{\max} \approx 2.0$ lacks any GISAXS scattering peaks, while the film swollen to $\varphi_{\max} \approx 1.6$ is found to exhibit distinct peaks in q_y but broad peaks in the q_z direction, as described above (regime v). Two further films, marked by red lines in Figure 3a, were brought into the ordered regime^[46] (i.e., regime iv) by slowly swelling to $\varphi_{\max} \approx 1.3$, as confirmed by the appearance of distinct, pronounced peaks in both q_y and q_z in the GISAXS patterns of the swollen state in Figure 3d,e.

A comparison of Figures 3b–e shows that it is beneficial to quench from the well-ordered swollen state at $\varphi_{\max} \approx 1.3$ compared to a higher swelling ratio. While all quenched films exhibit in-plane order with comparable peak-widths, only the samples quenched from $\varphi_{\max} \approx 1.3$ exhibit the full range of q_y and q_z peaks that can be confidently assigned to the alternating gyroid morphology based on indexing the corresponding GISAXS patterns (not shown; cf. Figure 1).

The line integral surfaces in Figure S1 (Supporting Information) and the corresponding quantitative analysis of the peak metrics in Figure S2 (Supporting Information) give further insight into quenching from differing φ_{\max} values. Focusing on the deswelling of the four samples, clear differences between the $\varphi_{\max} > 1.3$ and $\varphi_{\max} \approx 1.3$ samples emerge. For the former, an evolution in $q_y^{[110]}$ peak position and $\Delta q_y^{[110]}$ width is observed when quenching from φ_{\max} to $\varphi \approx 1.3$. In all samples the $q_y^{[110]}$ peak position does not change upon quenching below $\varphi \approx 1.3$ and the peak width increases only slightly. This indicates that two separate relaxation processes are active within the drying films and that the order that is present in the film for $\varphi \approx 1.3$ determines the order in the dry film. It appears that in the films quenched from $\varphi_{\max} > 1.3$, the sample did not have sufficient time to reorder, and their poor q_z order (Bragg rods rather than distinct reflections) is preserved in the dry films.

A quantitative analysis of the peak metrics (**Table 1** and Figure S2, Supporting Information) shows that films quenched from $\varphi_{\max} > 1.3$ lie at slightly higher q_y values compared to those quenched from $\varphi_{\max} \approx 1.3$, and they are somewhat narrower.

2.2.2. Solvent Removal Rate

Since slow quenching from high φ values is very time consuming, only two representative samples were explored. The similarity of the GISAXS patterns of the dried films in Figure 3b,c indicates that the solvent removal rate does not significantly affect the structure in the films that were quenched from $\varphi_{\max} > 1.3$. The two samples quenched from $\varphi_{\max} \approx 1.3$,

Table 1. Peak metrics (q_y peak positions and full widths at half maximum) corresponding to the dried film morphologies of ISO films annealed in the mixed vapors of THF and methanol (80:20), quenched from the disordered and microphase-separated swollen regimes at differing quenching rates.

Quench from $\varphi_{\max} \approx$	2.0	1.6	1.3	1.3
Quench rate [nm s ⁻¹]	4.59	1.07	1.69	0.21
$q_y^{[110]}$ [Å ⁻¹]	0.0261	0.0265	0.0255	0.0257
$\Delta q_y^{[110]}$ [$\times 10^{-4}$ Å ⁻¹]	5.40	6.30	7.72	7.40

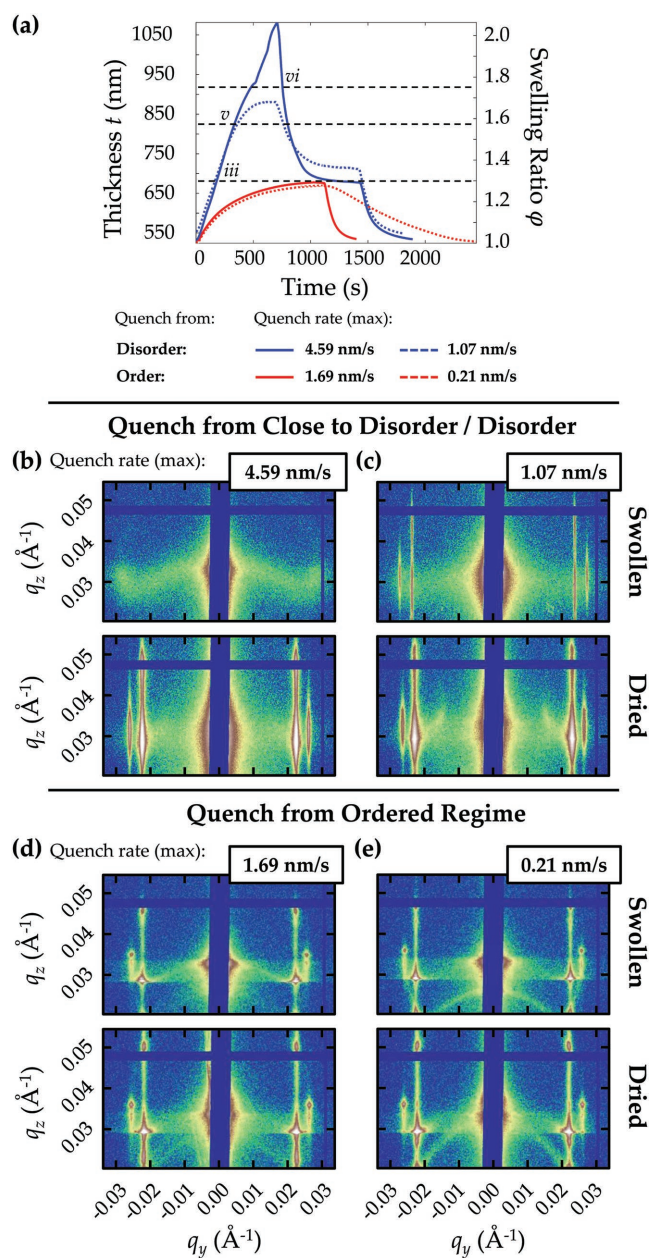


Figure 3. Effect of maximum swelling ratio and solvent removal rate on the dried film morphology. Film thickness profiles and GISAXS patterns of swollen and dried films subjected to different solvent removal (quench) rates after swelling to different maximal swelling ratios ϕ_{\max} . All films were annealed in mixed vapors of THF and methanol (80:20). a) Film thickness (swelling ratio) profiles of four films subjected to SVA. Two films were quenched from $\phi_{\max} > 1.3$ (blue lines) with maximal quench rates of 4.59 and 1.07 nm s⁻¹, respectively. Two further films were quenched from $\phi_{\max} \approx 1.3$ (red lines) with maximal solvent removal rates of 1.69 and 0.21 nm s⁻¹, respectively. The horizontal dashed lines correspond to the onset swelling ratios of SVA regimes found in Figure 2. b–e) GISAXS patterns ($\alpha_i = 0.18^\circ$) of the swollen (top row) and dried (bottom row) films for the four cases. The logarithmic color scales were normalized to the maximum and minimum intensities of each pattern.

on the other hand, maintain the distinct peak structure along the q_z direction (Figures 3d,e). This indicates that ϕ_{\max} is the dominant parameter, with the quench rate having only a minor influence on the organization of the microphase-separated morphology. This is borne out by the scattering peak parameters (Table 1 and Figures S2, Supporting Information), which are quantitatively similar for the samples quenched from $\phi_{\max} \approx 1.3$ and $\phi_{\max} > 1.3$, respectively.

2.3. Lattice Distortion upon Vitrification

Quenching a swollen film from the ordered regime maintains the alternating gyroid with a relatively high degree of in-plane order, as indicated by the results shown in Figure 3 (see above). However, a closer examination of the 3D structures reveals that the gyroid exhibits a significant distortion in the dried film. The corresponding changes of the 3D cubic lattice of the alternating gyroid upon drying were determined by indexing GISAXS patterns of swollen and dried ISO films (see the Experimental Section, cf. Figure 1). **Figure 4** shows indexed patterns of an ISO film annealed in a solvent vapor mixture of THF and methanol (50:50). The 2D peak patterns in the swollen (Figure 4a) and dried state (Figure 4b) look qualitatively similar and both were successfully indexed with the space group $I4_132$ (Q^{214}) of the alternating gyroid with the [110] direction oriented out-of-plane. However, only the swollen state structure shows a nearly ideal cubic unit cell ($a = b = 36.2$ nm, $c = 35.5$ nm, and $\gamma = 89^\circ$), whereas in the dried state the cubic lattice is significantly distorted. The unit cell of the dried film structure, $a = b = 32.6$ nm, $c = 36.0$ nm, and $\gamma = 101^\circ$, evidently deviates from a cubic lattice. Note that drying the films results in a decrease in a and b while c is found to increase. The changes of the lattice parameters upon drying correspond to a shrinkage of the unit cell along the [110] direction as schematically shown in Figure 4c. Note that similar effects were observed for ISO films annealed in varying compositions of mixed THF and methanol vapors (e.g., the effects of solvent vapor composition, see below).

2.4. Effect of Solvent Vapor Composition

In addition to the maximum swelling ratio and quench rate, the selectivity of the microphase-separated domains to the solvent vapor (or mixture of solvent vapors) is a further crucial SVA parameter which may affect the microphase-separated morphology, its long-range order, and effects related to vitrification of the polymer film. The SVA experiments presented above mainly used mixed solvent vapors of THF and methanol (80:20). The three PS, PI, and PEO microphase-separated domains are likely to exhibit different selectivities to the more polar methanol or the more apolar THF, which may lead to morphological transitions in the ISO terpolymer film. The effects of annealing in solvent vapors of different compositions on the swollen and dried microphase-separated morphologies were therefore investigated in **Figures 5–7**.

Figure 5 shows the GISAXS patterns of swollen (top row) and dried (bottom row) ISO films annealed in varying compositions of mixed THF and methanol vapors. The corresponding

Table 2. Maximum swelling ratio (ϕ_{\max}), approximate swelling ratio corresponding to the “ordering” regime (ϕ_{iii}), maximum swelling rate, and maximum quench rate for films annealed in THF and three THF and methanol mixtures (THF:MeOH).

	ϕ_{\max}	ϕ_{iii}	Swell rate [nm s ⁻¹]	Quench rate [nm s ⁻¹]
THF	1.54	1.20	1.11	0.99
THF:MeOH (90:10)	1.37	1.25	0.75	0.45
THF:MeOH (80:20)	1.27	1.24	0.63	0.69
THF:MeOH (50:50)	1.23	1.22	0.77	1.32

swelling and deswelling line integral surfaces are shown in Figure S4 (Supporting Information). All four swollen films have very similar GISAXS patterns with distinct peaks both in q_y and q_z in the swollen state. Upon drying, this pattern is retained in the films annealed in mixed solvent vapors of THF and methanol, but not in the film annealed in pure THF, where the peaks in q_z direction broadened significantly in the dried film. This deterioration of out-of-plane order probably arises from a swelling ratio much closer to the order–disorder transition ($\phi_{\max} \approx 1.54$, regime v), compared to the other samples (maximum swelling ratio $\phi_{\max} \approx 1.23$ – 1.37 , Table 2).

The lowest swelling ratio (ϕ_{iii}) at which the peak at $q_y \approx 0.026 \text{ \AA}^{-1}$ ($P_2 \sim q_y^{[110]}$; cf. Figure 2c) associated with the “ordering” regime (iii) appears for each of the samples in Figure 5 is given in Table 2. When comparing samples that were swollen with ϕ_{\max} sufficiently close to ϕ_{iii} , it is clear that the effect of the solvent mixing ratio is relatively small.

A careful analysis of the in-plane scattering peak metrics shown in Figure 6, however, reveals the detailed effects of

the solvent mixing ratio on the ISO microphase-separated morphology. Considering Figure 6b, it is clear that the $P_2 \sim q_y^{[110]}$ peak position decreases with increasing methanol content. But since the order–disorder transition (and hence the boundaries of the regimes described above) also vary with methanol content, it is difficult to disentangle thermodynamic and kinetic effects. It is therefore instructive to also consider the peak positions during swelling (Figure 6a). With increasing methanol content, the peak position $q_y^{[110]}$ becomes increasingly sensitive to the swelling ratio (i.e., the slope $dq_y^{[110]}/d\phi$ increases with increasing methanol content).

During swelling, the associated peak widths at $q_y \approx 0.026 \text{ \AA}^{-1}$ (i.e., $\Delta q_y^{[110]}$) follow a similar trend and narrow increasingly rapidly with increasing methanol content (Figure 6c), with the lowest absolute values for pure THF. This trend is much less evident in the deswelling curves of Figure 6d. Note that unlike the maximum swelling ratio, the maximum swell rate and quench rate of each of the films do not vary monotonically with the proportion of THF in the mixture of solvent vapors (Table 2).

The characteristics of the 3D lattice of the alternating gyroid in ISO films annealed in varying compositions of mixed THF and methanol vapors were determined by indexing of the GISAXS images in Figure 5 (cf. Figure 4). Figure 7 compares the drying-induced changes of the unit cell parameters of ISO films annealed in THF and three THF and methanol mixtures. In the swollen state, the unit cells are approximately cubic with an increasing deviation from an ideal cubic structure with increasing maximum swelling ratio (increasing methanol content) (Figure 7a,b). The smallest observed deviation from an ideal cubic unit cell (about 2%) is seen for a symmetric composition of THF and methanol (Figure 7c). In the dried films

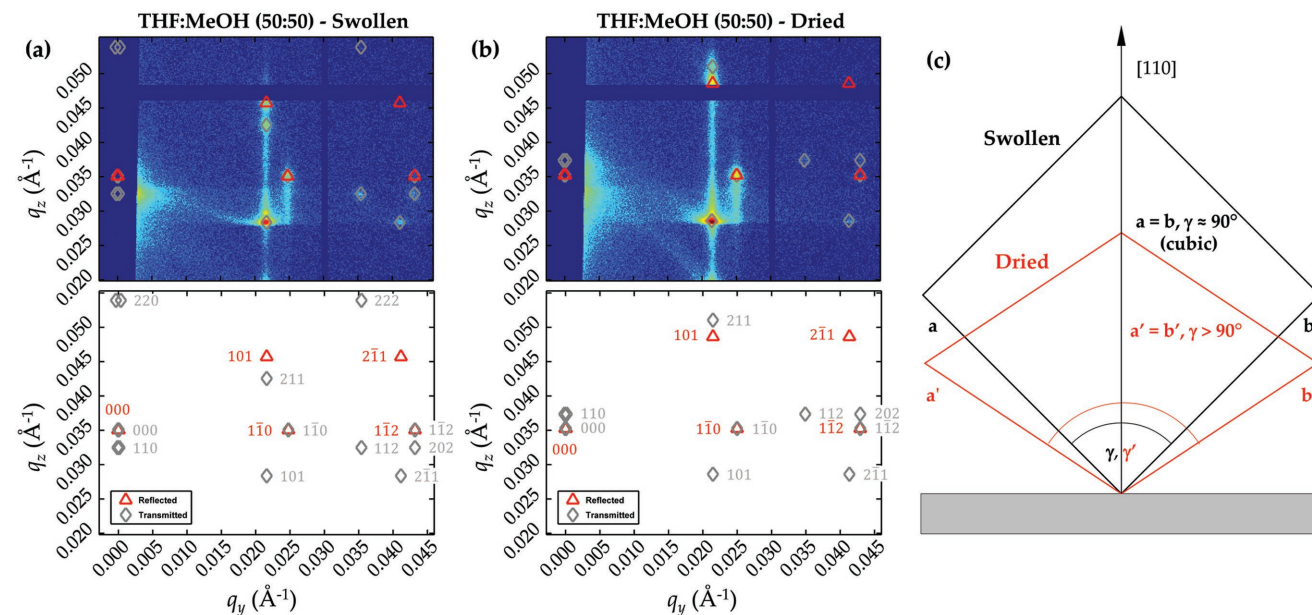


Figure 4. Vitrification-induced lattice distortion in solvent-annealed ISO films. Indexed 2D GISAXS patterns (top row) and corresponding reflections labeled with Miller indices (bottom row) of a) swollen and b) dried ISO films annealed in mixtures of THF and methanol (50:50). The indexed reflections correspond to peaks of the $I4_132$ space group with the [110] direction oriented perpendicular to the substrate using the following unit cell parameters: a) $a = b = 36.2 \text{ nm}$, $c = 35.5 \text{ nm}$, and $\gamma = 89^\circ$ for the swollen film, and b) $a = b = 32.6 \text{ nm}$, $c = 36.0 \text{ nm}$, and $\gamma = 101^\circ$ for the dried film. c) Schematic of the observed lattice changes in the [110] (out-of-plane) direction upon quenching.

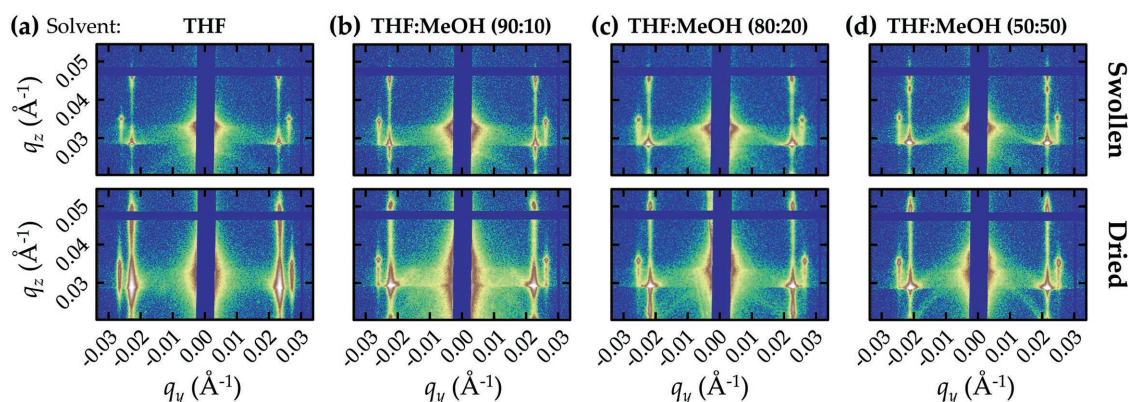


Figure 5. Effect of solvent vapor composition on the morphology of swollen and dried ISO thin films. GISAXS patterns ($\alpha_i = 0.18^\circ$) investigating the effect of solvent vapor composition on the swollen and dried microphase-separated morphologies of ISO films quenched from a) $\phi_{\max} \approx 1.6$ and b–d) $\phi_{\max} < 1.4$ (cf. Figure 2). The mixed solvent vapors used to anneal the films were a) THF, b) THF and methanol (THF:MeOH) (90:10), c) THF:MeOH (80:20), and d) THF:MeOH (50:50). The logarithmic color scales were normalized to the maximum and minimum intensities of each pattern.

the cubic unit cells are, however, significantly distorted for all THF and methanol mixing ratios (Figure 7a,b), again with the smallest effect ($a/c \approx 0.91$, Figure 7c) for the smallest maximum swelling ratio (the highest methanol content, THF:MeOH (50:50)). The distortion of the cubic lattice upon drying is schematically shown in Figure 4c. Note that such an out-of-plane distortion of the alternating gyroid is also observed in thermally annealed films, but to a much smaller extent ($a/c \approx 0.96$, $\gamma = 94^\circ$

after annealing at 160°C and subsequent quenching; Figure S3, Supporting Information).

3. Discussion

As in any annealing procedure, structure evolution by self-assembly is determined by the interplay of thermodynamic

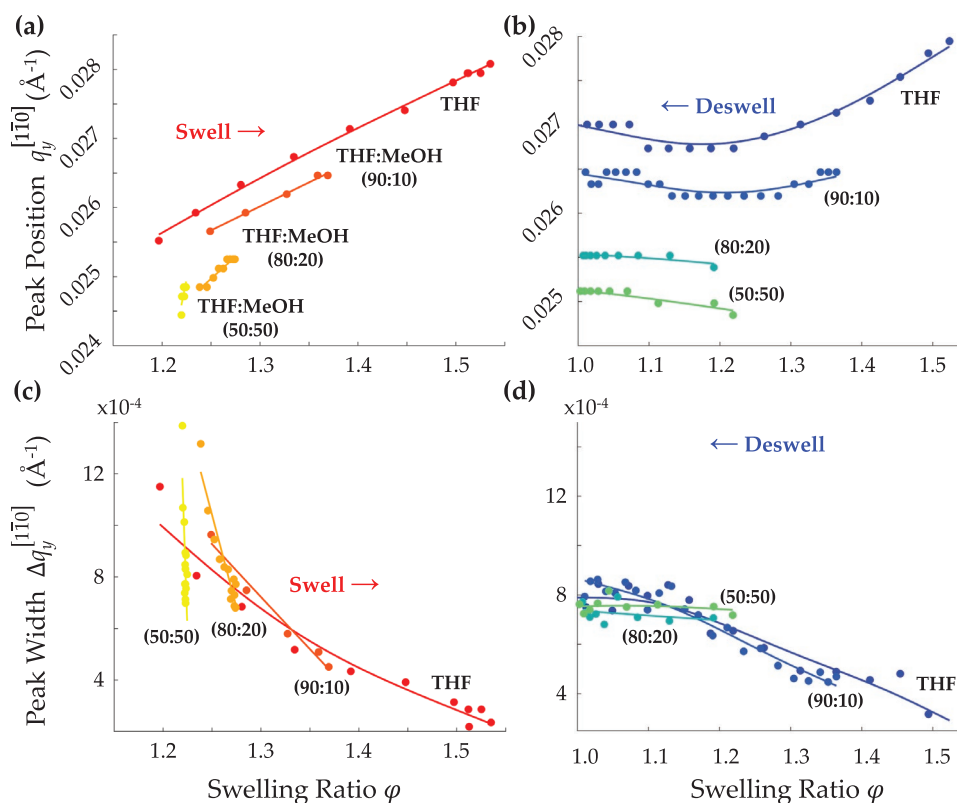


Figure 6. Effect of solvent vapor composition on the GISAXS peak positions and widths of ISO thin films during swelling and deswelling. Positions of the $q_y^{[110]} \approx 0.026 \text{ \AA}^{-1}$ peak (P_2) and their widths $\Delta q_y^{[110]}$ during a,c) swelling and b,d) deswelling of ISO thin films annealed in THF and three THF and methanol mixtures. The peak metrics were calculated from the corresponding GISAXS line integrals.

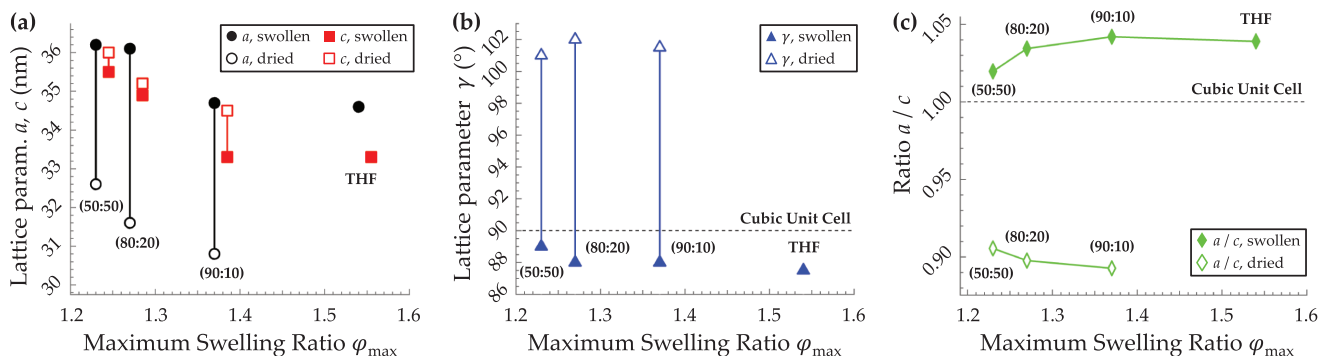


Figure 7. Effect of solvent vapor composition on lattice parameters of swollen and dried ISO thin films. Lattice parameters a) a and c , b) γ , and c) the ratio a/c of the ISO films annealed in THF and three THF and methanol mixtures in the swollen and dried films as a function of the maximum swelling ratio ϕ_{\max} . The lattice parameters were determined by indexing the 2D GISAXS images shown in Figure 5 and as demonstrated in Figure 4.

parameters (the path through phase space) and the kinetics of parameter evolution. In the case of SVA, this is further complicated by the varying overall volume: the solvent from the vapor phase is itself part of the thermodynamic system and influences the kinetics determined by the experimental protocol. The present study aims to improve our understanding of this complex system in the context of network-forming triblock terpolymers.

The as-spun film initially exhibits a kinetically trapped isotropic microphase-separated morphology with only short-range order.^[30] Upon plasticization due to solvent uptake, the film self-assembles towards its (solvated) equilibrium microphase-separated morphology (cf. Figure 2a). The ISO employed in this study, with its relative block lengths (see the Experimental Section) and the relative strength of the three Flory–Huggins interaction parameters ($\chi_{10} > \chi_{1s} \approx \chi_{s0}$), forms an alternating gyroid in both thermally annealed bulk samples^[27] and the solvent-annealed films studied here (Figure 1a–c). In the ISO alternating gyroid, the PI and PEO blocks form the two interpenetrating single gyroid networks separated by the continuous matrix of the PS block (Figure 1d). Since the PS matrix is glassy at room temperature—while PI and PEO both are well above their respective glass transition temperatures—ISO plasticization is governed by the solvent uptake of PS. As the solvent concentration in the film increases, the degree of order of the alternating gyroid morphology improves, both in- and out-of-plane. Using the Scherrer equation,^[47] i.e., $\Delta d = K \times 2\pi / \Delta q_y^{[110]}$, where $K \approx 0.93$, the lateral grain size is $\Delta d \approx 0.63 \mu\text{m}$ upon ordering, improving to $\Delta d \approx 2.40 \mu\text{m}$ before disordering.^[48] At the same time, the gyroid lateral unit cell size (i.e., $d = \sqrt{2} \times 2\pi / q_y^{[110]}$) decreases as the swelling ratio is increased, from 34.8 nm upon ordering to a minimum of 31.8 nm just below the order–disorder transition. This decrease in lateral unit cell size points to a solvent-mediated reduction in the three Flory–Huggins interaction parameters at high swelling ratios, and therefore a reduction in the net segregation strength of the terpolymer. Note that the simultaneous swelling of the film with a reduction in unit cell size implies a substantial reorganization of the gyroid morphology, since the number of gyroid lattice unit cells has to significantly increase to reconcile a simultaneous increase in film thickness with a (small) reduction in the lattice constants. **Figure 8a,b** schematically shows this structural reorganization, which is similar to

the swelling (and deswelling) of cylindrical^[12] and lamellar^[40,49] morphologies.

As the solvent concentration is further increased, order in the alternating gyroid morphology begins to deteriorate in the out-of-plane direction while it continues to improve in the plane. Since there is very little change in the $q_y^{[110]}$ signal, part of the film remains an ordered gyroid. At the same time, another part of the film, most likely layers at one or both film surfaces, loses the gyroid morphology and transforms to either i) a disordered morphology, ii) an ordered morphology that is not periodic in 3D (e.g., lamellae), or iii) into a mixed state. Morphological surface reorganization upon approaching the order–disorder transition is not surprising, since with the three Flory–Huggins interaction parameters continuing to decrease, surface interactions become increasingly important.

Upon deswelling from disorder, the alternating gyroid morphology reappears and the lateral unit cell size once again increases until the onset of vitrification at a unit cell size of 34.1 nm. Although significantly improved compared to the as-spun film, the dry film has a lower degree of order compared to the swollen film, both in- and out-of-plane (cf. Figure 2e), with a lateral grain size in the dried film of $\approx 1.08 \mu\text{m}$. This much lower degree of order arises again from the substantial morphological reorganization imposed on the terpolymer morphology. The drying of the film causes a simultaneous volume reduction and increase in the three Flory–Huggins parameters requiring a significant reduction in number of gyroid unit cells in the out-of-plane direction. However, the increase in film viscosity with decreasing solvent content slows down the reorganization of the gyroid lattice and suppresses it entirely once the PS matrix is vitrified. This slowing-down and freezing-in of the continuously reorganizing microphase-separated morphology results in the observed decreased order within the vitrified film.

The kinetics of the structural reorganization is seen in the GISAXS line integral plots of Figure 2c. During swelling, both the peak position $q_y^{[110]}$ and width $\Delta q_y^{[110]}$ vary monotonically (approximately linearly) with the swelling ratio. The variation of $q_y^{[110]}$ and $\Delta q_y^{[110]}$ during deswelling resemble that of the swelling plot (albeit with a different slope) for swelling ratios above $\phi \approx 1.3$. However, both quantities vary very little upon further solvent removal for $\phi < 1.3$. This indicates the existence of two different quenching regimes, where for $\phi > 1.3$ the morphology

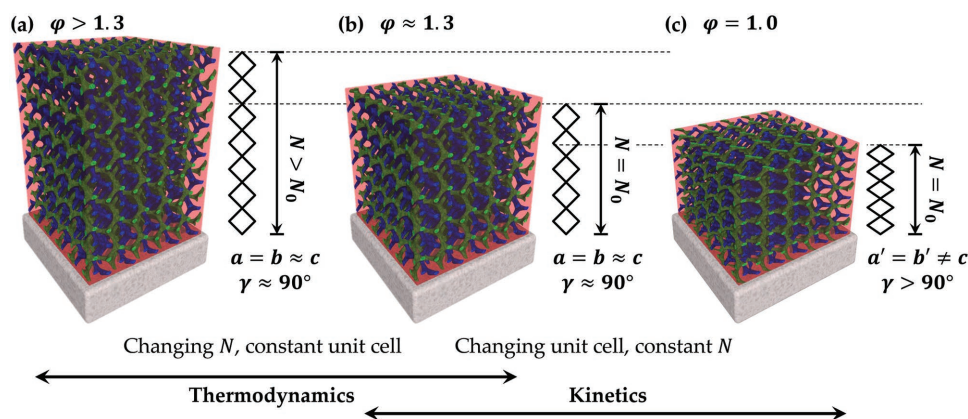


Figure 8. Structural changes in ordered gyroid terpolymer films during SVA. In the ordered regimes, two scenarios for structural changes are found. a,b) Close to and above the plasticization regime, $\phi \approx 1.3$, changes in swelling ratio lead to a structural reorganization involving a change in the number of unit cells, N , in the direction perpendicular to the substrate, during which the cubic nature of the gyroid is maintained ($a = b \approx c$, $\gamma \approx 90^\circ$). c) Below $\phi \approx 1.3$, deswelling, vitrification, and the accompanied thickness reduction result in a distortion of the gyroid unit cell in the out-of-plane direction ($a = b \neq c$, $\gamma > 90^\circ$) without changing the number of unit cells.

is sufficiently mobile to allow the continuous reorganization of the microphase-separated morphology upon change in swelling ratio, while for $\phi < 1.3$ the microphase-separated morphology is essentially immobile (cf. Figure 8). As a consequence, the gyroid morphology freezes in before the film is completely dried. This discrepancy between the kinetics of structural reorganization and drying creates a problem. As the film thickness continues to decrease during the drying process, the already-vitrified gyroid morphology ($\phi < 1.3$) begins to distort in the out-of-plane direction as illustrated in Figure 8c. This results in a significant out-of-plane distortion ($\approx 10\%$) of the cubic lattice of the alternating gyroid in dried films as shown in Figure 4. A drying-induced lattice distortion was observed previously in solvent annealed diblock copolymer films exhibiting double gyroid, spherical, cylindrical, or lamellar morphologies.^[18] Upon significant vertical shrinkage, spherical morphologies were found to undergo a transition from a body-centered cubic to a face-centered orthorhombic lattice.^[17,50]

In this context, it is instructive to revisit two different quenching conditions. A rapid quench from a swollen film with $\phi_{\max} \gg 1.3$ preserves the high degree of in-plane order and the smaller lateral unit-cell size of the swollen gyroid (i.e., kinetically arresting morphological reorganization during deswelling). Unfortunately, the small degree of out-of-plane order is also preserved. On the other hand, annealing the sample at $\phi \approx 1.3$ allows the system to attain a reasonable in- and out-of-plane order, which changes only little upon quenching. A variation of the quench rate does not seem to play an important role, neither for quenching from $\phi > 1.3$ nor from $\phi \approx 1.3$. A very slow quench from $\phi \approx 1.3$, however, improves the order somewhat.

Clearly, these two cases illustrate a compromise when designing SVA protocols for gyroid terpolymer films with the aim of achieving long-range order both in and out of the plane of the film. High swelling ratios are required for optimal in-plane order but this comes at the expense of potentially poorer out-of-plane order, i.e., the film does not have the same microphase-separated morphology across its entire thickness. Equilibrating the films at a “sweet-spot” swelling ratio (here

$\phi \approx 1.3$), on the other hand, enables good out-of-plane order but at the expense of the in-plane order of the microphase-separated morphology (cf. Figure 3 and Table 1). For perpendicular lamellae or perpendicular cylinders, where only the in-plane order is relevant, annealing close to the order–disorder transition is found to optimize the degree of ordering.^[11,51]

Varying the ratio of the THF and methanol in the solvent vapor mixture adds a further degree of freedom to the experimental parameter space. Given the strong selectivity of methanol for PEO, the insensitivity of the results of Figure 5 is surprising. Selective swelling of one of the domains often leads to morphological transitions, as found for example in diblock copolymers.^[18,20] The lack of such a transition in the ISO triblock terpolymer system arises from the relatively large composition window in the ISO phase diagram for which the alternating gyroid morphology is reported. This is in sharp contrast to the narrow double gyroid region in the phase diagram of diblock copolymers.^[23,52] Clearly, the molecular composition of the ISO used in this study places its equilibrium morphology firmly within alternating gyroid phase space, as indeed intended (see the Experimental Section).^[53]

Since the swelling of the ISO film is governed by the PS matrix phase, the main effect of the THF and methanol ratio lies in the maximum swelling ratio attainable for a given flow rate of solvent vapor and temperatures of sample and solvent, which decreases markedly with increasing methanol content. This has a strong effect on the swollen ISO unit cell size. Since the unit cell size is typically frozen-in during the quench (see above), as shown previously in cylindrical BCP thin films,^[12] the main effect of the solvent composition lies in the final gyroid lattice constant. The in-plane order, as measured through the peak width $\Delta q_y^{(110)}$, is affected very little by the THF and methanol ratio.

4. Conclusion

This study investigates in detail the phase behavior of a gyroid-forming ISO triblock terpolymer upon swelling and quenching from a THF and methanol solvent vapor atmosphere. The

system can be described in eight morphological swelling and deswelling regimes that straddle the dry film and a mixed ISO “solution” film. Attempts to equilibrate the ISO morphology in the swollen state and preserve its order in the quenched film are fundamentally limited by the thermodynamic requirement of the polymer to readjust its microphase-separated morphology with the swelling ratio. Within the 3D network morphology, this requires diffusive transport of the chains, which becomes increasingly difficult (from both a thermodynamic and kinetic point of view) as the sample is quenched.

Two scenarios were found, which present the experimenter with a conundrum. Quenching from a highly swollen state (either ordered or disordered) results in a high degree of lateral (in-plane) order, but the film is not ordered across its entire thickness. Quenching from a less swollen microphase-separated state, exhibiting order both in- and out-of-plane across the entire film, allows to retain the microphase-separated morphology with 3D order in the dried film, but at expense of a high degree of in-plane order. The dominant control parameter for this is the maximum swelling ratio, with the swelling and quench rates modifying the microphase-separated morphology only very little within the range of parameters explored. The experiments further reveal a significant distortion of the cubic unit cell in dried films in the out-of-plane direction (i.e., the “direction of drying”), a fundamental obstacle toward achieving true 3D order in solvent-annealed gyroid films.

These results contribute toward the rational design of SVA protocols for the successful fabrication of large grains of the alternating gyroid morphology in triblock terpolymers, for example for 3D optical metamaterial^[5,6,54,55] applications. The robustness of the alternating gyroid morphology with respect to all varied SVA parameters is of great benefit as it ensures that the gyroid morphology is remarkably robust with respect to the SVA protocol. This robustness is likely one of the reasons why gyroid grain sizes of hundreds of micrometers could be generated in ISO terpolymer films of higher molecular weight, although detailed SVA protocols have not been reported.^[14] While the gyroid grain sizes achieved in this study were still limited to micrometer range, the protocols explored suggests possible improvements. For example, oscillating the sample between different swelling ranges, or designing a staged deswelling protocol, may provide ways to improve lateral order and limit out-of-plane distortion without sacrificing the morphology spanning the film.

5. Experimental Section

Polymer Films: The polyisoprene-*b*-polystyrene-*b*-poly(ethylene oxide) (ISO) triblock terpolymer with a total molecular weight of 33 kg mol⁻¹ was prepared by anionic polymerization following synthesis procedures reported elsewhere.^[56,57] The block volume fractions of the terpolymer were $f_{PI} = 0.31$, $f_{PS} = 0.52$, and $f_{PEO} = 0.17$. Thin films of the ISO terpolymer were prepared atop silicon substrates which were cleaned by exposure to an oxygen plasma (Diener MRC 100 at 100 W power for 2 min). Thin films were spun from a 10% (w/w) solution of ISO terpolymer in anhydrous anisole (Sigma-Aldrich) for 60 s at 1200 rpm with an acceleration of 500 rpm s⁻¹. The resulting film thickness was 520–560 nm as determined by thin film interferometry (see below).

PI and PS with number-average molecular weights of 103 kg mol⁻¹ (polydispersity of 1.07) and 103 kg mol⁻¹ (polydispersity of 2.5),

respectively, were purchased from Polymer Source. PEO with a number-average molecular weight of 100 kg mol⁻¹ was purchased from Sigma-Aldrich (Merck). Homopolymer films were prepared by spin coating a 10% (w/w) solution of the respective homopolymer in anhydrous anisole (Sigma-Aldrich) onto silicon substrates (cleaned as above) for 60 s at 3200 rpm with an acceleration of 500 rpm s⁻¹. The resulting film thicknesses were 542 ± 7 nm (PI), 762 ± 12 nm (PS), and 989 ± 6 nm (PEO).

Solvent Vapor Annealing: The samples were exposed to controlled amounts of solvent vapor using a custom-made annealing chamber. The PEEK annealing chamber had sealed Kapton windows on two opposing sides (for transmission of the incident and scattered X-ray beams) and a sealed quartz glass window in the lid (for measurement of the film thickness during annealing). Three gas lines were joined and the mixed gas flowed into and through the chamber, creating a well-defined solvent atmosphere within it: dry nitrogen flowed through one of the three lines, while for the other two the dry nitrogen was bubbled through various solvents. By controlling the volume flow rate in each line with three independently controlled mass flow controllers (MKS Type MF1, flow range 100 sccm, MKS Type 647 multichannel gas flow controller unit), the ratio of solvent-saturated to dry nitrogen (i.e., the “concentration” of the—potentially mixed—solvent vapor) flowing into the chamber was controlled. Custom-built software (written in Python) controlled the flow rates to adjust the desired solvent vapor concentration in the chamber, enabling the implementation of predetermined solvent annealing protocols.

THF and methanol (Sigma-Aldrich) were employed as solvents. Unless otherwise noted, the combined mass flow rate was maintained at 20 sccm throughout the experiments. Upon exiting the chamber, the gas mixture flowed into an exhaust line through a manual mass flow controller which could be adjusted to ensure the maintenance of a sufficiently high solvent vapor pressure in the annealing chamber. The temperature of the sample within the annealing chamber was controlled using a Peltier element mounted on a copper plate, and the solvent reservoirs were immersed in a temperature-controlled water bath (ThermoFisher ARCTIC SC150-A10B Refrigerated Circulator). Unless otherwise noted, the temperature of the solvent was held at ≈23.0 °C, while the temperature of the sample was varied between ≈21.3 and 24.4 °C, depending on the required swelling ratio (a lower sample temperature resulting in greater swelling). The temperature of the solvent was set to a value close to room temperature (≈23.7 °C) to avoid condensation of solvent in the gas lines. The ambient relative humidity was constant at ≈33%.

In an attempt to determine the selectivity of THF and methanol mixture vapors for the respective blocks of ISO terpolymer, the swelling behavior of PS, PI, and PEO homopolymer films was characterized by monitoring their relative thickness increase upon exposure to saturated solvent vapor atmospheres (Table 3). The temperature of the samples was kept at ≈21 °C and the relative humidity was ≈45–60%. PEO did not exhibit any significant swelling regardless of the solvent vapor used, which is probably related to the semicrystalline nature of homopolymer PEO at room temperature. However, the swelling data for PS and PI reveal a selectivity of THF for PI, and an increasing selectivity of the THF and methanol mixtures for PS with increasing methanol content.

Film Thickness Measurements: The thickness of the terpolymer films during solvent vapor annealing was measured interferometrically in situ using an Avantes AvaLight-DH-S-BAL deuterium halogen light source (only the halogen source, with its 500–2500 nm wavelength range, was

Table 3. Ratios of swollen to dry film thicknesses of ISO terpolymer and corresponding homopolymer films annealed in saturated atmospheres of THF and a THF and methanol mixture (THF:MeOH).

	PS	PI	PEO	ISO
THF	1.37	1.42	1.06	1.36
THF:MeOH (80:20)	1.48	1.36	1.06	1.42

employed) and an Avantes AvaSpec 2048L spectrometer (the effective wavelength range measured was 500–1000 nm). Light was coupled through a bifurcated optical fiber (FCR-12UV200/600-2-ME) and focused onto the sample via a collimator (FCR-COL UV/VIS). The thickness was estimated by assuming a refractive index of $n = 1.5$ for the terpolymer film. The swelling ratio is a dimensionless measure of relative film thickness and is defined as

$$\varphi = \frac{t}{t_0} \quad (1)$$

where t is the swollen thickness and t_0 the initial thickness of the as-spun film (i.e., before application of any solvent). Assuming no in-plane motion of the film during annealing, the swelling ratio is the reciprocal of the volume fraction of polymer in the swollen film.

In Situ Grazing-Incidence Small-Angle X-Ray Scattering: GISAXS measurements were performed in situ during solvent vapor annealing at the cSAXS beamline of the Swiss Light Source, Paul Scherrer Institute, Villigen, Switzerland. The X-ray energy was 11.2 keV and the sample-to-detector distance was 7232.5 mm, determined by calibration with a silver behenate standard. Scattering patterns were recorded on a PILATUS 2M detector with a 1 s exposure time at incident angles in the $\alpha_i = 0.14^\circ$ – 0.18° range. To avoid damaging the terpolymer film by X-ray overexposure, the film was laterally translated by 250 μm prior to each measurement (e.g., after the previous measurement and any alignment protocols).

GISAXS Indexing: Indexing of the 2D GISAXS patterns was performed using the GIXSGUI software (version 1.6.4) in Matlab.^[58] All GISAXS images were successfully indexed with the reflections of the $I4_132$ space group with the [110] direction oriented perpendicular to the substrate, Miller indices in h, k, l range of -2 to 2 , and unit cell parameters in the following ranges: 30.8–36.2 nm for a and b , 33.3–36.0 nm for c , 87.5 – 102° for α and γ . The critical angle α_c and the incident angle α_i were varied in the $\alpha_c = 0.107$ – 0.110° and $\alpha_i = 0.173$ – 0.179° range, respectively.

GISAXS In-Plane Analysis: GISAXS scattering patterns were reduced using *Nika*,^[59] a software package for IGOR Pro 6 (WaveMetrics), and the in-plane line integrations were subsequently analyzed using custom software to automatically determine peak locations and widths as a function of the swelling ratio. Peaks $[hkl]$ were analyzed by fitting the composite function

$$I(q_y) = I_0 + I_1 q_y^{-d} + \sum_{n=1}^N \frac{I_{[hkl]}^{(n)}}{1 + \left(\frac{q_y - q_{y(n)}^{[hkl]}}{\Delta q_{y(n)}^{[hkl]}} \right)^2} \quad (2)$$

to the spectra, where I_0 , I_1 , d , $I_{[hkl]}^{(n)}$, and $\Delta q_{y(n)}^{[hkl]}$ were varied, and $q_{y(n)}^{[hkl]}$ was fixed during the fitting procedure. Peak positions $q_{y(n)}^{[hkl]}$ were determined prior to fitting by a peak-finding algorithm. The values of the peak widths $\Delta q_{y(n)}^{[hkl]}$ resulted from the fit. Zero ($N = 0$), one ($N = 1$), or two ($N = 2$) Lorentzian peaks were identified during fitting.

Atomic Force Microscopy: Solvent-annealed ISO terpolymer films were imaged using an Asylum Research Cypher AFM (Oxford Instruments) operated in tapping mode using uncoated silicon probes with a cantilever force constant of 85 N m^{-1} , a resonance frequency of 1600 kHz, and a tip radius of about 7 nm.

Supporting Information

Supporting Information is available from the Wiley Online Library or from the author. Additional data related to this publication is available at the University of Cambridge data repository at: <https://doi.org/10.17863/CAM.26377>.

Acknowledgements

This project has received funding from the European Union's Horizon 2020 research and innovation programme under the Marie Skłodowska-Curie grant agreement no. 706329/cOMPoSe (I.G.). This research was

also supported through the Swiss National Science Foundation through grant numbers 163220 (U.S.) and 168223 (B.D.W.), the National Center of Competence in Research Bio-Inspired Materials (U.S., B.D.W., I.G.), the Adolphe Merkle Foundation (B.D.W., U.S., I.G.), the Engineering and Physical Sciences Research Council through the Cambridge NanoDTC EP/G037221/1, EP/L027151/1, and EP/G060649/1 (R.D., J.A.D., J.J.B.), and ERC LINASS 320503 (J.J.B.). U.W. (DMR-1707836) and M.S. (DMR-1752615) thank the National Science Foundation for financial support. The authors further acknowledge the Paul Scherrer Institut, Villigen, Switzerland for provision of synchrotron radiation beamtime at beamline X12SA (cSAXS) of the SLS and would like to thank Ana Diaz for assistance during the GISAXS experiments. Part of the work presented here was carried out with the support of the Diamond Light Source, beamline I22 (proposal SM13448). The authors also acknowledge Oxford Instruments for granting access to their Cypher ES AFM and would like to thank Ted F. Limpoco (Oxford Instruments) for his support during AFM measurements.

Conflict of Interest

The authors declare no conflict of interest.

Keywords

block copolymer self-assembly, gyroids, in situ grazing-incidence small-angle X-ray scattering (GISAXS), solvent vapor annealing, triblock terpolymers

Received: June 22, 2018

Revised: July 20, 2018

Published online:

- [1] F. H. Schacher, P. A. Rugar, I. Manners, *Angew. Chem., Int. Ed.* **2012**, *51*, 7897.
- [2] R. Ruiz, H. Kang, F. A. Detcheverry, E. Dobisz, D. S. Kercher, T. R. Albrecht, J. J. de Pablo, P. F. Nealey, *Science* **2008**, *321*, 936.
- [3] C.-H. Lin, S. Polisetty, L. O'Brien, A. Baruth, M. A. Hillmyer, C. Leighton, W. L. Gladfelter, *ACS Nano* **2015**, *9*, 1379.
- [4] C. M. Bates, M. J. Maher, D. W. Janes, C. J. Ellison, C. G. Wilson, *Macromolecules* **2014**, *47*, 2.
- [5] S. Vignolini, N. A. Yufa, P. S. Cunha, S. Guldin, I. Rushkin, M. Stefik, K. Hur, U. Wiesner, J. J. Baumberg, U. Steiner, *Adv. Mater.* **2012**, *24*, OP23.
- [6] J. A. Dolan, M. Saba, R. Dehmel, I. Gunkel, Y. Gu, U. Wiesner, O. Hess, T. D. Wilkinson, J. J. Baumberg, U. Steiner, B. D. Wilts, *ACS Photonics* **2016**, *3*, 1888.
- [7] K. Hur, Y. Francescato, V. Giannini, S. A. Maier, R. G. Hennig, U. Wiesner, *Angew. Chem. Inter. Ed.* **2011**, *50*, 11985.
- [8] P. W. Majewski, K. G. Yager, *J. Phys.: Condens. Matter* **2016**, *28*, 403002.
- [9] E. Kim, H. Ahn, S. Park, H. Lee, M. Lee, S. Lee, T. Kim, E.-A. Kwak, J. H. Lee, X. Lei, J. Huh, J. Bang, B. Lee, D. Y. Ryu, *ACS Nano* **2013**, *7*, 1952.
- [10] S. Park, Y. Kim, H. Ahn, J. H. Kim, P. J. Yoo, D. Y. Ryu, *Sci. Rep.* **2016**, *6*, 36326.
- [11] A. Baruth, M. Seo, C. H. Lin, K. Walster, A. Shankar, M. A. Hillmyer, C. Leighton, *ACS Appl. Mater. Interfaces* **2014**, *6*, 13770.
- [12] X. Gu, I. Gunkel, A. Hexemer, W. Gu, T. P. Russell, *Adv. Mater.* **2014**, *26*, 273.
- [13] X. Gu, I. Gunkel, A. Hexemer, T. P. Russell, *Macromolecules* **2016**, *49*, 3373.
- [14] R. Dehmel, J. A. Dolan, Y. Gu, U. Wiesner, T. D. Wilkinson, J. J. Baumberg, U. Steiner, B. D. Wilts, I. Gunkel, *Macromolecules* **2017**, *50*, 6255.

- [15] C. Sinturel, M. Morris, M. A. Hillmyer, *Macromolecules* **2013**, *46*, 5399.
- [16] D. Posselt, J. Zhang, D.-M. Smilgies, A. V. Berezkin, I. I. Potemkin, C. M. Papadakis, *Prog. Polym. Sci.* **2017**, *66*, 80.
- [17] M. Y. Paik, J. K. Bosworth, D.-M. Smilgies, E. L. Schwartz, X. Andre, C. K. Ober, *Macromolecules* **2010**, *43*, 4253.
- [18] M. A. Chavis, D. M. Smilgies, U. B. Wiesner, C. K. Ober, *Adv. Funct. Mater.* **2015**, *25*, 3057.
- [19] I. Gunkel, X. Gu, Z. Sun, E. Schaible, A. Hexemer, T. P. Russell, *J. Polym. Sci., B* **2016**, *54*, 331.
- [20] A. V. Berezkin, F. Jung, D. Posselt, D. Smilgies, C. M. Papadakis, *Adv. Funct. Mater.* **2018**, *28*, 1706226.
- [21] M.-S. She, T.-Y. Lo, R.-M. Ho, *Macromolecules* **2014**, *47*, 175.
- [22] Y.-H. Wu, T.-Y. Lo, M.-S. She, R.-M. Ho, *ACS Appl. Mater. Interfaces* **2015**, *7*, 16536.
- [23] F. S. Bates, G. H. Fredrickson, *Phys. Today* **1999**, *52*, 32.
- [24] A. J. Meuler, M. A. Hillmyer, F. S. Bates, *Macromolecules* **2009**, *42*, 7221.
- [25] F. S. Bates, M. F. Schulz, A. K. Khandpur, S. Forster, J. H. Rosedale, K. Almdal, K. Mortensen, *Faraday Discuss.* **1994**, *98*, 7.
- [26] A. K. Khandpur, S. Foerster, F. S. Bates, I. W. Hamley, A. J. Ryan, W. Bras, K. Almdal, K. Mortensen, *Macromolecules* **1995**, *28*, 8796.
- [27] T. H. Epps, E. W. Cochran, C. M. Hardy, T. S. Bailey, R. S. Waletzko, F. S. Bates, *Macromolecules* **2004**, *37*, 7085.
- [28] T. H. Epps, E. W. Cochran, T. S. Bailey, R. S. Waletzko, C. M. Hardy, F. S. Bates, *Macromolecules* **2004**, *37*, 8325.
- [29] R. J. Albalak, M. S. Capel, E. L. Thomas, *Polymer* **1998**, *39*, 1647.
- [30] G. Kim, M. Libera, *Macromolecules* **1998**, *31*, 2569.
- [31] J. N. L. Albert, W.-S. Young, R. L. Lewis, T. D. Bogart, J. R. Smith, T. H. Epps, *ACS Nano* **2012**, *6*, 459.
- [32] J. E. Seppala, R. L. Lewis, T. H. Epps, *ACS Nano* **2012**, *6*, 9855.
- [33] H. Elbs, C. Drummer, V. Abetz, G. Krausch, *Macromolecules* **2002**, *35*, 5570.
- [34] K. Fukunaga, H. Elbs, R. Magerle, G. Krausch, *Macromolecules* **2000**, *33*, 947.
- [35] K. Fukunaga, T. Hashimoto, H. Elba, G. Krausch, *Macromolecules* **2003**, *36*, 2852.
- [36] A. Ségolène, A. Karim, M. Muhammad, T. Siham, P. Gilles, W. Anne-Laure, B. Cyril, C. Eric, F. Guillaume, H. Georges, *Macromol. Rapid Commun.* **2018**, *39*, 1800043.
- [37] A. Karim, M. Muhammad, A.-F. Alberto, M. Jean, A. Ségolène, P. Gilles, P. Virginie, D. Cécile, F. Guillaume, H. Georges, *Macromol. Rapid Commun.* **2018**, *39*, 1700754.
- [38] C. K. Shelton, T. H. Epps, *Polymer* **2016**, *105*, 545.
- [39] W. Bai, K. G. Yager, C. A. Ross, *Macromolecules* **2015**, *48*, 8574.
- [40] Z. Di, D. Posselt, D. M. Smilgies, C. M. Papadakis, *Macromolecules* **2010**, *43*, 418.
- [41] Z. Di, D. Posselt, D. M. Smilgies, R. Li, M. Rauscher, I. I. Potemkin, C. M. Papadakis, *Macromolecules* **2012**, *45*, 5185.
- [42] Q. Zhang, F. Matsuoka, H. S. Suh, P. A. Beaucage, S. Xiong, D.-M. Smilgies, K. W. Tan, J. G. Werner, P. F. Nealey, U. Wiesner, *ACS Nano* **2018**, *12*, 347.
- [43] The onset swelling ratios corresponding to regimes *ii-iv* depend on the swelling rate, as chain motion and thus ISO self-assembly are kinetically limited at low solvent concentrations due to slow chain diffusion close to the plasticization regime.
- [44] B. Lee, I. Park, J. Yoon, S. Park, J. Kim, K.-W. Kim, T. Chang, M. Ree, *Macromolecules* **2005**, *38*, 4311.
- [45] T. P. Lodge, B. Pudil, K. J. Hanley, *Macromolecules* **2002**, *35*, 4707.
- [46] Note that the swelling rate applied here is much smaller than in Figure 2, which likely results in lower onset swelling ratios of regimes *ii-iv*, and thus allowing a well-ordered structure to form slightly below the onset swelling ratio of the ordered regime in Figure 2.
- [47] D.-M. Smilgies, *J. Appl. Crystallogr.* **2009**, *42*, 1030.
- [48] Note that this estimate does not take the instrument-related peak broadening into account. The given values are therefore lower bound estimates.
- [49] A. A. Rudov, E. S. Patyukova, I. V. Neratova, P. G. Khalatur, D. Posselt, C. M. Papadakis, I. I. Potemkin, *Macromolecules* **2013**, *46*, 5786.
- [50] J. Bosworth, M. Paik, R. Ruiz, E. Schwartz, J. Huang, A. Ko, D. Smilgies, C. Black, C. Ober, *ACS Nano* **2008**, *2*, 1396.
- [51] S. Hur, V. Thapar, R. Abelardo, G. Khaira, S. Tamar, R. P. A. W. Li, M. Müller, P. F. Nealey, J. J. de Pablo, *Proc. Natl. Acad. Sci. USA* **2015**, *112*, 14144.
- [52] F. S. Bates, G. H. Fredrickson, *Annu. Rev. Phys. Chem.* **1990**, *41*, 525.
- [53] J. Chatterjee, S. Jain, F. S. Bates, *Macromolecules* **2007**, *40*, 2882.
- [54] S. Salvatore, A. Demetriadou, S. Vignolini, S. S. Oh, S. Wuestner, N. A. Yufa, M. Stefik, U. Wiesner, J. J. Baumberg, O. Hess, U. Steiner, *Adv. Mater.* **2013**, *25*, 2713.
- [55] J. A. Dolan, B. D. Wilts, S. Vignolini, J. Baumberg, U. Steiner, *Adv. Opt. Mater.* **2015**, *3*, 12.
- [56] T. S. Bailey, H. D. Pham, F. S. Bates, *Macromolecules* **2001**, *34*, 6994.
- [57] T. S. Bailey, C. M. Hardy, T. H. Epps, F. S. Bates, *Macromolecules* **2002**, *35*, 7007.
- [58] Z. Jiang, *J. Appl. Crystallogr.* **2015**, *48*, 917.
- [59] J. Ilavsky, *J. Appl. Crystallogr.* **2012**, *45*, 324.